Proceedings of ICFDP7:
Seventh International Congress On Fluid Dynamics & Propulsion
December 18-20, 2001, Cairo, Egypt

ICFDP7-2001019

NUMERICAL SIMULATION OF OPEN ROTOR NOISE

Ashraf S. Sabry
Assoc. Professor
Mechanical Power Engineering Dept.
Cairo University

John K. Kamel
Research Assistant
Mechanical Power Engineering Dept
Cairo University

Mahmoud A. Fouad
Professor
Mechanical Power Engineering.Dept.
Cairo University

ABSTRACT

A numerical simulation for the noise generation and propagation from an open rotor with subsonic and supersonic tip speed is presented. The model proposed by Tam [1] has been used to present the sound generation from the rotor.

The linearized Euler Equations (LEE) have been discretized by the MacCormack (2-4) scheme of Gottlieb and Turkel [2], which is fourth order in space and second order in time.

Special attention was given to the boundary treatment. Radiation boundary treatment developed by Tam et al. [3] was used to prevent reflections of spurious waves.

The effects of the change of the tip speed have been studied. Diagrams for the pressure, velocity, sound pressure level and directivity of radiated sound have been plotted to illustrate differences between the studied cases.

Comparisons with asymptotic solution of Tam [1] as well as the numerical solution of Tam and Aganin [4] and Fang Hu [5] have illustrated the accuracy of the present solution in spite of the limitation of the used computational domain.

Keywords : open rotor, noise, computational aeroacoustics, CAA, acoustics

INTRODUCTION

Recently, Tam and Aganin [6] used the Dispersion-Relation-Preserving (DRP) scheme with radiation boundary conditions to solve the open rotor noise problem.

The model that he has solved includes the effect of the force exerted by the rotor on the fluid. He used a grid with a mesh size of 0.02 in the source region. Such high resolution was not needed far from the source region, thus a multiple-size-mesh multiple-time-step DRP algorithm was used.

Moreover, Tam [1] has introduced the asymptotic solution in order to validate his numerical solution. The asymptotic solution has enabled him to get the sound directivity as the radius of the spherical sound wave approaches infinity. Tam and Aganin [6] has used a relatively large computational domain of radius 50 in order to compare between the sound directivity obtained from both the asymptotic and numerical solutions.

On the other hand, Fang Hu [5] solved the same problem by using the Low-Dissipation and Low-Dispersion Runge-Kutta Scheme (LDDRK56). Moreover, he applied a tenth-order explicit filter throughout his relatively small computational domain and used Perfectly Matched Layer (PML) equations at the non-reflecting boundaries

The present work is concerned with numerical simulation of fan noise. The governing equations used are the Linearized form of Euler's Equations. Special attention has been given to boundary treatment to avoid contaminating the

solution with spurious modes resulting from the reflection at the boundaries.

The comparison of the present study with Tam and Aganin [4], Fang Hu [5] and the asymptotic solution of Tam [1] showed that the MacCormack (2-4) scheme is capable of getting accurate results despite the limitations of the used computational domain.

NOMENCLATURE

b	Blade length
$\bar{c}_0$	Speed of sound
D	Directivity of sound
F_x, F_r, F_ϕ	Body force components in x, r, ϕ direction, respectively
F	Flux in the axial direction
G	Flux in the radial direction
J_m	Bessel function of order m^{th}
L_x, L_r, $L\phi$	Operators in axial, radial and azimuthal directions, respectively
M	Mach number
m	Number of rotor blades
p`	Wave pressure
P_{rms}	Root-mean-square pressure
Q	Unknown variable
R	Distance from the origin of the coordinate system measured
S	Source term
SPL	Sound pressure Level (dB)
t	Time
Δt	Time step
u',v',w'	Wave velocities in x, r, and ϕ direction respectively
x, r, ϕ	Streamwise, radial, and azimuthal coordinate
θ	Emission angle
ρ_∞	Ambient gas density
Ω	Angular velocity = fan tip speed

GOVERNING EQUATIONS

Following the open rotor noise problem as presented in the 3rd CAA benchmark problems [1], the nondimensional variables are defined with respect to the following scales.

length scale = b (blade length)

velocity scale = $\bar{c}_0$ (ambient sound speeed)

time scale = $\dfrac{b}{\bar{c}_0}$

density scale = ρ_∞ (ambient gas density) (1)

pressure scale = $\rho_\infty \bar{c}_0^2$

body force scale (per unit volume) = $\dfrac{\rho_\infty \bar{c}_0^2}{b}$

The rotor exerts a rotating force on the fluid. As a model problem, the rotor effect is replaced by a rotating body force. Hence, the governing linearized Euler Equations in cylindrical coordinates (x, r, ϕ) will be in the following form:

$$\frac{\partial v'}{\partial t} = -\frac{\partial p'}{\partial r} + F_r$$

$$\frac{\partial w'}{\partial t} = -\frac{1}{r}\frac{\partial p'}{\partial \phi} + F_\phi \qquad (2)$$

$$\frac{\partial u'}{\partial t} = -\frac{\partial p'}{\partial x} + F_x$$

$$\frac{\partial p'}{\partial t} + \frac{1}{r}\frac{\partial (v'r)}{\partial r} + \frac{1}{r}\frac{\partial w'}{\partial \phi} + \frac{\partial u'}{\partial x} = 0$$

Where (F_r , F_ϕ , F_x) are the components of body force.

For simplicity, it was assumed that $F_r = 0$. While $F\phi$ and F_x take the following form:

$$\begin{bmatrix} F_\phi(r,\phi,x,t) \\ F_x(r,\phi,x,t) \end{bmatrix} = Re\left\{ \begin{bmatrix} \tilde{F}_\phi(r,x) \\ \tilde{F}_x(r,x) \end{bmatrix} e^{im(\phi-\Omega t)} \right\} \qquad (3)$$

Where $Re\{\ \}$ is the real part. For computation purposes, the following body force distribution in r & x directions is used:

$$\tilde{F}_\phi(r,x) = \begin{cases} h(x) r J_m(\lambda_{mN} r) & r \le 1 \\ 0 & r > 1 \end{cases} \qquad (4)$$

$$\tilde{F}_x(r,x) = \begin{cases} h(x) J_m(\lambda_{mN} r) & r \le 1 \\ 0 & r > 1 \end{cases} \qquad (5)$$

$$h(x) = exp\left\{-(ln\,2)(10x)^2\right\} \qquad (6)$$

Where $J_m(\ )$ is the m^{th} order Bessel Function and λ_{mN} is the N^{th} root of $J'_m(\lambda_{mN}) = 0$. In this model, m is the number of blades and Ω is the angular velocity of the rotor.

It was possible to reduce the 3-dimensional problem of (2) to a two-dimensional problem by factoring out the azimuthal dependence by letting

$$\begin{bmatrix} u'(r,\phi,x,t) \\ v'(r,\phi,x,t) \\ \omega'(r,\phi,x,t) \\ p'(r,\phi,x,t) \end{bmatrix} = Re\left\{ \begin{bmatrix} \tilde{u}(r,x,t) \\ \tilde{v}(r,x,t) \\ \tilde{\omega}(r,x,t) \\ \tilde{p}(r,x,t) \end{bmatrix} e^{im\phi} \right\} \qquad (7)$$

The governing equations for $(\tilde{u},\tilde{v},\tilde{\omega},\tilde{p})$ are deduced by substituting (3) to (7) into (2) and factoring out $e^{im\emptyset}$,thus :

$$\frac{\partial \tilde{v}}{\partial t} = -\frac{\partial \tilde{p}}{\partial r}$$

$$\frac{\partial \tilde{w}}{\partial t} = -\frac{im}{r}\tilde{p} + \tilde{F}_\phi(r,x)e^{-im\Omega t}$$

$$\frac{\partial \tilde{u}}{\partial t} = -\frac{\partial \tilde{p}}{\partial x} + \tilde{F}_\chi(r,x)e^{-im\Omega t} \qquad (8)$$

$$\frac{\partial \tilde{p}}{\partial t} + \frac{1}{r}\frac{\partial(\tilde{v}r)}{\partial r} + \frac{im\tilde{w}}{r} + \frac{\partial \tilde{u}}{\partial x} = 0$$

These Equations could be written in a conservative form as:

$$\frac{\partial Q}{\partial t} + \frac{\partial F}{\partial x} + \frac{1}{r}\frac{\partial(rG)}{\partial r} = \frac{1}{r}S \qquad (9)$$

where,

$$Q = \begin{bmatrix} \tilde{v} \\ \tilde{w} \\ \tilde{u} \\ \tilde{p} \end{bmatrix} \qquad (10)$$

$$F = \begin{bmatrix} 0 \\ 0 \\ \tilde{p} \\ \tilde{u} \end{bmatrix} \qquad (11)$$

$$G = \begin{bmatrix} \tilde{p} \\ 0 \\ 0 \\ \tilde{v} \end{bmatrix} \qquad (12)$$

$$S = \begin{bmatrix} \tilde{p} \\ -im\tilde{p} + r\tilde{F}_\phi(r,x)e^{-im\Omega t} \\ r\tilde{F}_x(r,x)e^{-im\Omega t} \\ -im\tilde{w} \end{bmatrix} \qquad (13)$$

COMPUTATIONAL GRID

In the present work two different computational grids have been used. The first grid as shown in figure (1) has been used for subsonic tip speed 0.85. Using 301 points, the grid extends axially from (x/b= -8.8) to (x/b = 8.8). With a total of 300 points in the radial direction, the grid stands just above the centerline at (r/b=0.02) and extends to (r/b=17.68). The grid spacing is stretched both in the axial and radial directions as the location from the source is increased.

The second grid, which has been used for supersonic tip speed of 1.15, is shown in figure (2). Using 403 points, the grid extends axially from (x/b= -8.805) to (x/b = 8.805). It also extends in the radial direction to about half the extent of the first grid.

NUMERICAL ALGORITHM

In the present work, the Macormack (2-4) scheme due to Gottlieb and Turkel [2], that is second order accurate in time and fourth order accurate in space, is used. This scheme is an extension of the classical, second order accurate Macormack (2-2) scheme. Sankar et al. [7] have evaluated this scheme for aeroacoustics applications.

The operator is split into separate radial and axial contributions.

$$Q^{n+2} = L_x L_r L_r L_x Q^n \qquad (14)$$

Each operator consists of a predictor and a corrector step. Each step uses one-sided difference:

Predictor

$$Q^{n+1/2} = Q^n - \frac{\Delta t}{6\Delta x}(7F_i - 8F_{i-1} + F_{i-2})^n \qquad (15)$$

Corrector

$$Q^{n+1} = \frac{1}{2}[Q^n + Q^{n+\frac{1}{2}} + \frac{\Delta t}{6\Delta x}(7F_i - 8F_{i+1} + F_{i+2})^{n+\frac{1}{2}}] \qquad (16)$$

and likewise for the radial direction. To avoid any numerical biasing of the solution the sweep directions are reversed between operators:

$$Q^{n+2} = L_x^{+-} L_r^{+-} L_r^{-+} L_x^{-+} Q^n \qquad (17)$$

At the computational boundaries flux quantities from outside the computational domain are required for the spatial differences. These quantities are computed using third order accurate extrapolations from the interior of the domain:

$$F_{i+1} = 4F_i - 6F_{i-1} + 4F_{i-2} - F_{i-3} \qquad (18)$$

$$F_{i+2} = 4F_{i+1} - 6F_i + 4F_{i-1} - F_{i-2} \qquad (19)$$

BOUNDARY TREATMENT

Special attention is given here into boundary treatment in order to avoid nonphysical oscillations that can render the computed oscillating field unacceptable. The boundary treatments used were found to be stable, non-reflecting and suitable for the present computations as illustrated in Figure (3).

RADIATION BOUNDARY CONDITIONS

In the radiation boundary condition, the conventional acoustic radiation conditions apply:
Where,

$$Q_t = -V \left[\frac{x}{R} Q_x + \frac{r}{R} Q_r + \frac{Q}{R} \right] \quad (20)$$

$$R = \sqrt{x^2 + r^2} \quad (21)$$

$$V = \bar{c} \left[\frac{x}{R} M + \sqrt{1 - \left(\frac{r}{R} M \right)^2} \right] \quad (22)$$

Where M is the local Mach number.

The spatial derivatives that appear in equation (20) are computed in an identical manner as inner flow derivatives.

CENTERLINE TREATMENT

For Bessel functions of integer order, the solution can be extended into the region of negative argument as:

$$J_m(-r) = (-1)^m J_m(r) \quad (23)$$

By means of equation (23), the solution may be extended to the negative r part of the x-r plane as follows,

$$\tilde{u}(-r,x) = (-1)^m \tilde{u}(r,x)$$

$$\tilde{v}(-r,x) = (-1)^{m-1} \tilde{v}(r,x)$$

$$\tilde{w}(-r,x) = (-1)^{m-1} \tilde{w}(r,x) \quad (24)$$

$$\tilde{p}(-r,x) = (-1)^m \tilde{p}(r,x)$$

So for even m values it becomes an axisymmetric problem, where at the centreline :

$$\frac{\partial}{\partial r} \begin{Bmatrix} \tilde{u} \\ \tilde{p} \end{Bmatrix} = 0 \quad (25)$$

$$\tilde{v} = 0 \quad (26)$$

$$\tilde{w} = 0 \quad (27)$$

To implement this boundary condition numerically, the fluxes are projected to ghost points across the centerline in an appropriate manner.

RESULTS

The numerical results of the acoustic field of an 8 blades open rotor are investigated in detail for two cases, a subsonic rotor tip speed of 0.85 and a supersonic rotor tip speed of 1.15.

For subsonic case, figures (4), (5), (6) & (7) represent a snap shot of pressure, radial velocity, azimuthal velocity and axial velocity respectively.Figures (8) & (9) illustrate the root mean square of pressure and sound pressure level respectively.

Figure (10) & (11) represent the distribution of root mean square of pressure and sound pressure level along (x/b=0) line respectively, whereas figure (12) illustrates the pressure history at point (0,5) as a function of time.

For supersonic case, figure (13) & (14) represent the distribution of root mean square of pressure and sound pressure level along (x/b=0) line respectively, whereas figure (15) illustrates the pressure history at point (0,5) as a function of time.

Figure (16) & (17) illustrate the comparisons between the present and previous works for the directivity of the sound.

where,

$$D(\theta) = \lim_{R \to \infty} R^2 \left(\overline{p`^2(R,\theta,\phi,t)} \right)$$

and $\left(\overline{\quad} \right)$ is the time average.

CONCLUSION

By comparing the asymptotic and previous numerical solutions with the present work, it is possible to conclude that the present numerical scheme and boundary treatment were capable to reach reasonable results despite the limitation of the present computational domain.

REFERENCES

[1]Tam, C.K.W., " Rotor Noise: Catrgory 2, Analytical Solution ", 2000, Proceedings of the Third Computational Aeroacoustics Workshop on Benchmark Problems, NASA CP-2000-209790, pp. 41-46.

[2] Gottlieb, D., and Turkel, E., 1976, "Dissipative Two-Four Methods for Time-Dependent problems", Mathematics of Computation, Vol. 30, pp.703-723.

[3]Tam, C.K.W, Fanh, J., and Kurbatskil, K. A., 1996, "Inhomogeneous Radiation Boundary Conditions Simulating Incoming Acoustic Waves for Computational Aero-Acoustics", Proceedings of the International Congress on Fluid Mechanics & Propulsion, Cairo, Egypt, pp. 332-339

[4] Tam, C.K.W., and Aganin, A., 2000, "Comparisons with Asymptotic Solution: Category 2", Proceedings of the Third Computational Aeroacoustics Workshop on Benchmark Problems", NASA CP-2000-209790, pp.401-402.

[5] Fang Q. Hu, 2000, "Results of Benchmark Problems for the Third Computational Aeroacoustics Workshop" Proceedings of the Third Computational Aeroacoustics Workshop on Benchmark Problems", NASA CP-2000-209790, pp. 169-189.

[6]Tam, C.K.W., and Aganin, A., 2000, "Computation of Transonic and Rotor Problems by the Dispersion-Relation-Preserving Scheme" Proceedings of the Third Computational Aeroacoustics Workshop on Benchmark Problems, NASA CP-2000-209790, pp. 191-202.

[7] Sankar, L.N., Reddy . N.N., and Hariharan, N., 1993, "A Comparative Study of Numerical Schemes for Aero-acoustic Application", in Computational Aero-and Hydro-Acoustics. (EDS Mankbadi et al..), FED-Vol.147, pp.35-40

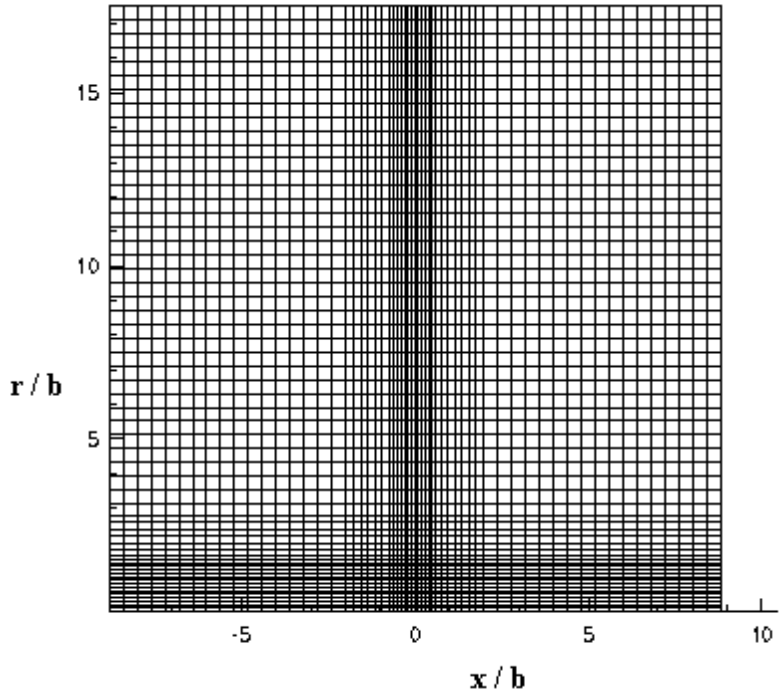

Figure (1) Computational Grid (1)

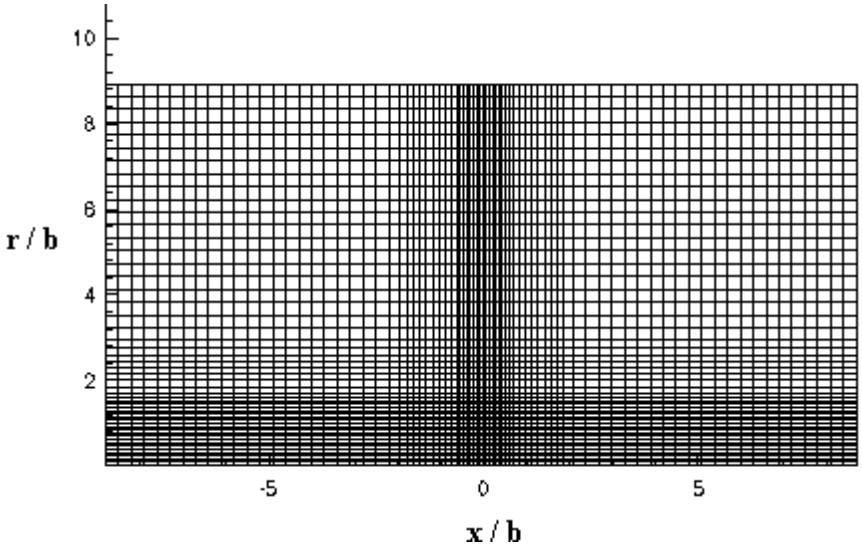

Figure (2) Computational Grid (2)

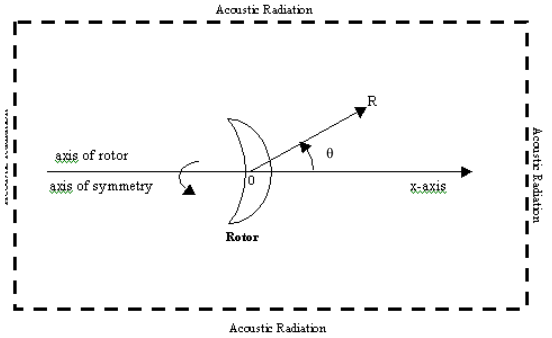

Figure (3) Computational Domain

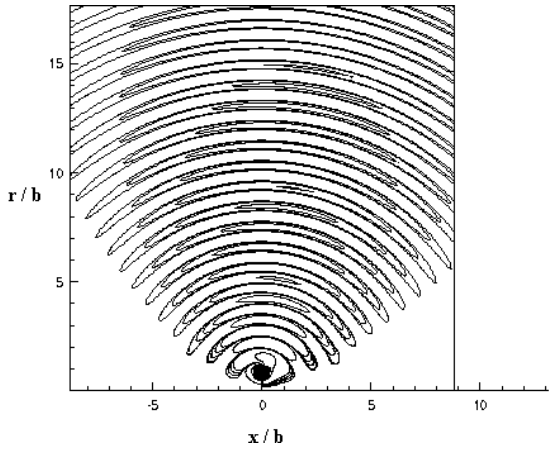

Figure (4) Snap Shot of the Pressure Disturbance Field (Ω=0.85, m=8)

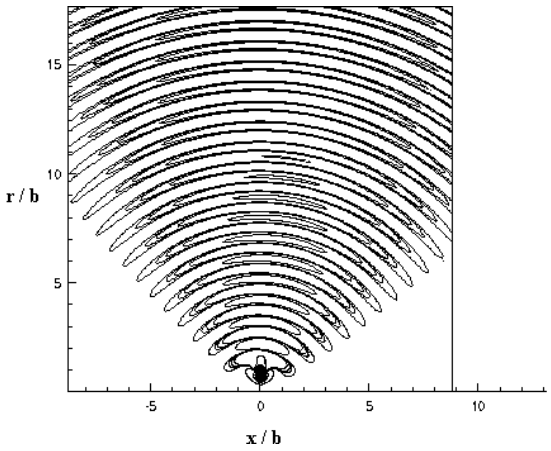

Figure (5) Snap Shot of the Radial Velocity Disturbance Field (Ω=0.85, m=8)

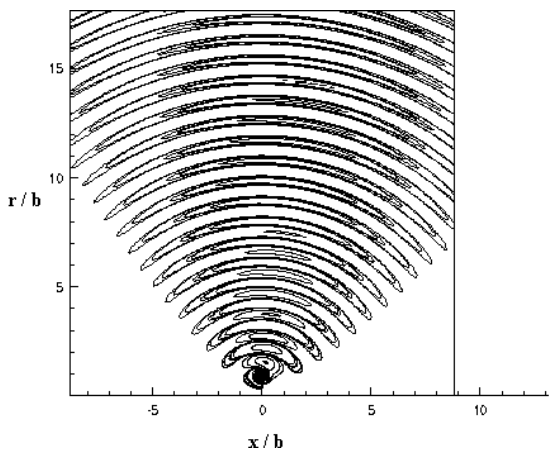

Figure (6) Snap Shot of the Azimuthal Velocity Disturbance Field (Ω=0.85, m=8)

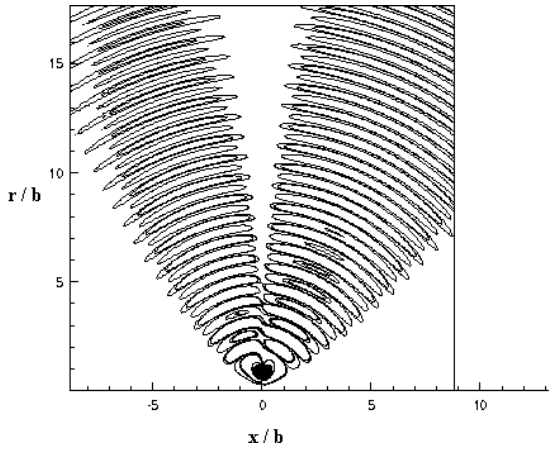

Figure (7) Snap Shot of the Axial Velocity Disturbance Field (Ω=0.85, m=8)

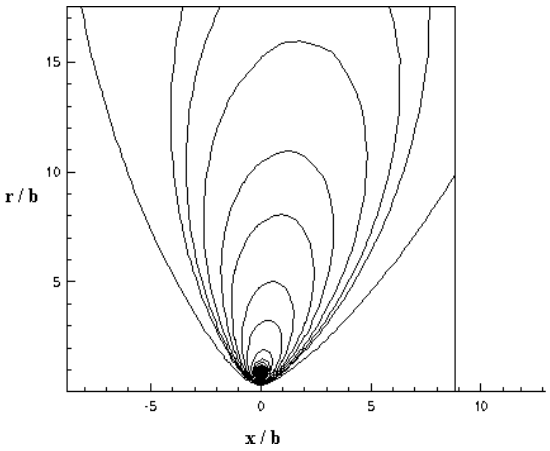

Figure (8) Root-Mean-Square Pressure Contours (Ω=0.85, m=8)

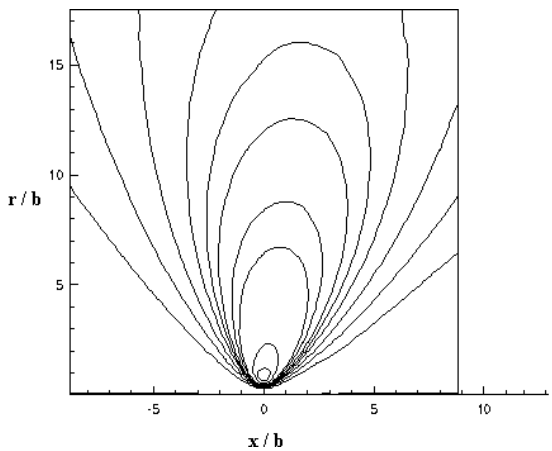

Figure (9) Sound Pressure Level Contours (Ω=0.85 , m=8)

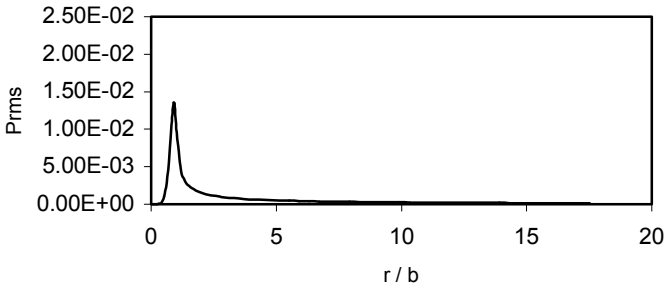

Figure (10) Root-Mean-Square Pressure Distribution along x/b=0 line (Ω=0.85 , m=8)

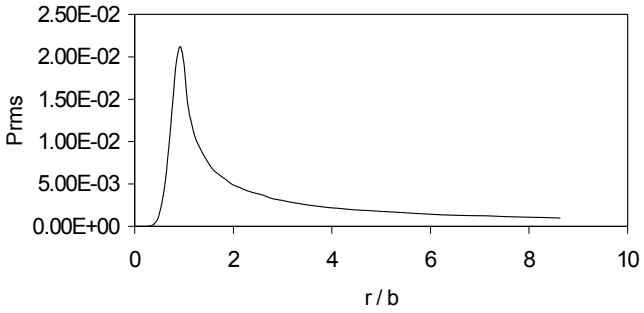

Figure (13) Root-Mean-Square Pressure Distribution along x/b=0 line (Ω=1.15, m=8)

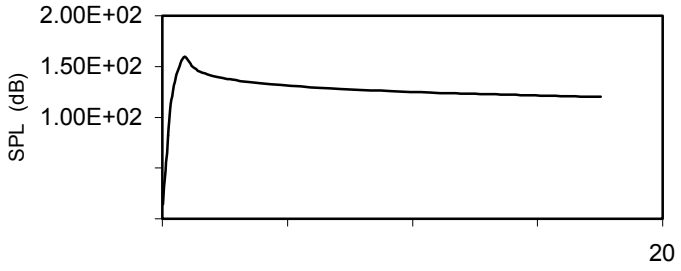

Figure (11) Sound Pressure Level Distribution along x/b=0 line (Ω=0.85 , m=8)

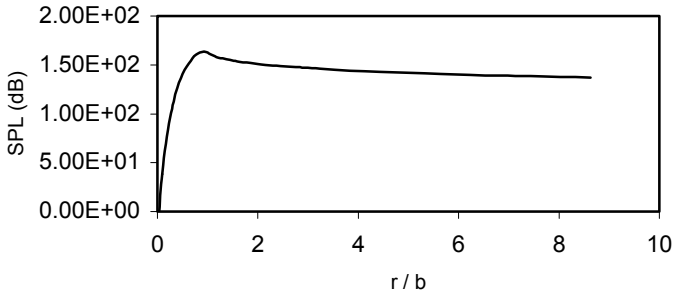

Figure (14) Sound Pressure Level Distribution along x/b=0 line (Ω=1.15 , m=8)

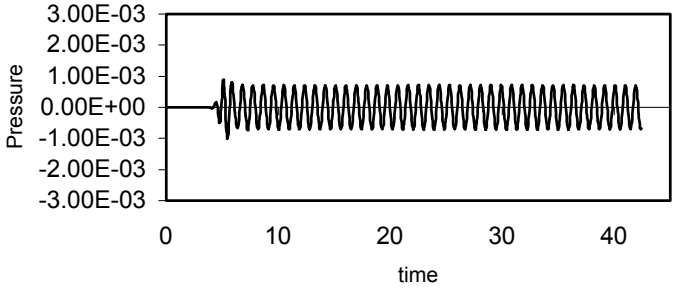

Figure (12) Sound Pressure as a Function of Time at point (0,5.0) (Ω=0.85 , m=8)

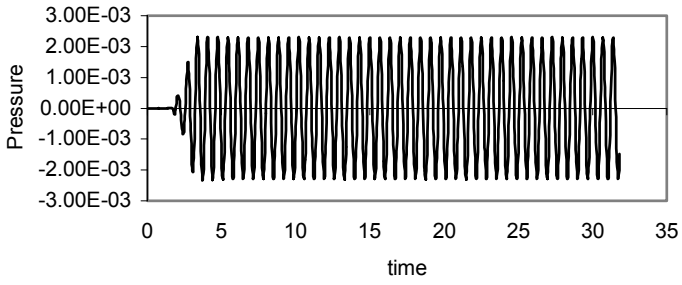

Figure (15) Sound Pressure as a Function of Time at point (0,5.0) (Ω=1.15, m=8)

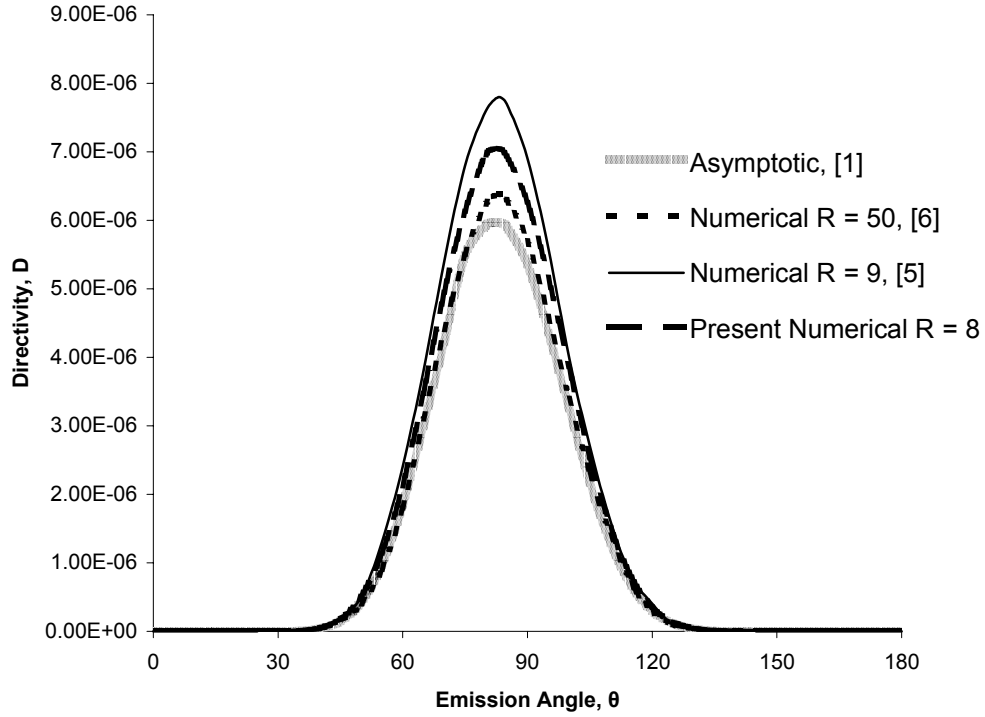

Figure (16) Comparison between present and previous works for the Directivity of Radiated Sound (Ω=0.85, m=8)

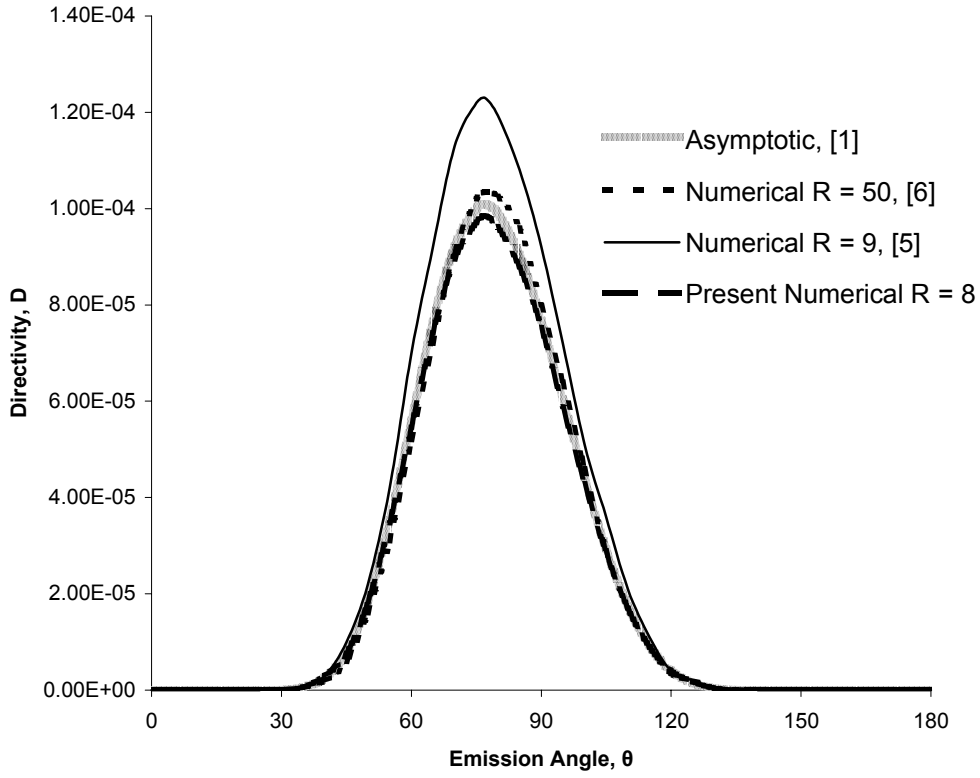

Figure (17) Comparison between present and previous works for the Directivity of Radiated Sound (Ω=1.15, m=8)